JTTEE5 14:187-195
DOI: 10.1361/10599630523746
1059-9630/$19.00 © ASM International

Parametric Study of an HVOF Process for the Deposition of Nanostructured WC-Co Coatings

Cecilia Bartuli, Teodoro Valente, Fabio Cipri, Edoardo Bemporad, and Mario Tului

(Submitted September 22, 2003; in revised form November 4, 2003)

Nanocrystalline WC-Co coatings were deposited by high velocity oxyfuel from commercial nanostructured composite powders. Processing parameters were optimized for maximal retention of the nanocrystalline size and for minimal decarburation of the ceramic reinforcement. Thermochemical and gas-dynamical properties of gas and particle flows within the combustion flame were identified in various operating conditions by computational fluid-dynamics (CFD) simulation. Significant improvements of the mechanical properties of the coatings were obtained: a decrease of the friction coefficient was measured for the nanostructured coatings, together with an increase of microhardness and fracture toughness.

Keywords computational fluid-dynamics, decarburation, HVOF, nanostructured, WC-Co, wear resistance

1. Introduction

Composite chromium carbide-nickel chrome, tungsten carbide-cobalt, and other cermet coatings for wear-resistant applications in the mechanical, aeronautic, and naval fields are typically deposited by high velocity oxyfuel (HVOF) spraying (Ref 1). In particular, tungsten carbide reinforced cobalt and cobalt-chrome deposits have been proposed and tested as hard chrome replacement candidates for aircraft landing gears and hydraulic rods, ball valves in the oil industry, anilox print rolls, etc. (Ref 2, 3).

Improved performance in terms of surface hardness and tribological properties can be expected from the use of nanocrystalline coatings (Ref 4-8) as a direct consequence of the extremely high density of grain boundaries characterizing this class of materials. However, due to the higher reactivity and grain growth sensitivity of nanostructured ceramic reinforcements, the exposure to high temperature oxidizing flames must be minimized, while guaranteeing the formation of dense and homogeneous deposits.

The present research was focused in the study of a liquid fuel HVOF process for the deposition of nano-WC reinforced 15% cobalt matrix coatings. Optimization of the spraying process was carried out using a statistical design of experiments on the basis of the results of microstructural and mechanical characterization of the coatings. For a critical assessment of the spraying conditions and of their influence on the degradation of the nanostructured carbides, a computational fluid-dynamic model (CFD) (Ref 9-12) was set up for the simulation of the properties of combustion gas and WC-Co powders inside an HVOF JP-5000 torch and in the external section of the combustion flame.

Cecilia Bartuli, Teodoro Valente, and **Fabio Cipri,** Department of Chemical and Materials Engineering, University of Rome "La Sapienza" Rome, Italy; **Edoardo Bemporad,** Department of Mechanical and Industrial Engineering, University "Roma Tre" Rome, Italy; and **Mario Tului,** CSM Rome, Italy. Contact e-mail: bartuli@uniroma1.it.

2. Materials and Methods

The spraying equipment used for the experimental campaigns in the present work was a liquid fuel HVOF apparatus (JP-5000, Tafa Inc., Praxair Surface Technologies, Concord, NH) burning a kerosene-oxygen mixture.

Computational fluid-dynamic simulation of the thermochemical and gas-dynamical properties of the combustion gas and of the sprayed particles in the combustion flame was implemented using the FLUENT 5.4.8 solver (Fluent Inc., Lebanon, NH). The geometrical models and the reference grids were generated using a commercial preprocessor software (GAMBIT 1.3, Fluent Inc., Lebanon, NH). A k-ε model (Ref 13) (k represents the turbulent kinetic energy and ε its dissipation rate) was used to describe turbulence phenomena. A finite rate chemistry (Ref 14) model was used to solve the transport equations for reagents and products. Equilibrium stoichiometric coefficients of molecular and dissociated species were calculated at the experimental pressure (about 8 atm) using a commercial monodimensional chemical code (GASeq: chemical equilibria for perfect gases, release 0.63, free software available at http://www.c.morley.ukgateway.net). Eddy dissipation concept (EDC) (Ref 13) was applied to analyze the influence of turbulence on the chemistry of the combustion flame. More details about the simulation codes, the adopted equations, and the assumed simplificative conditions can be found in Ref 15.

The gas pressure built up inside the combustion chamber was measured by a pressure-gage positioned at the combustor inlet. The temperature and feed rate of the cooling water were monitored during spraying.

Nanostructured WC-15 wt.% Co powders (Nanocarb, Union Miniere, NJ; nucleated and coprecipitated by spray conversion with a specified carbide size of < 50 nm) were used as feedstock materials for nanocrystalline coatings: particle size distribution of these powders was characterized by laser granulometry (Malvern Mastersizer, Malvern Instruments Ltd., Malvern, Worcestershire, UK), and Rosin-Rammler parameters were calculated accordingly. Particle size distribution is illustrated in Fig. 1(a); the average size of the particles is about 48 μm.

Conventional coatings were deposited from agglomerated

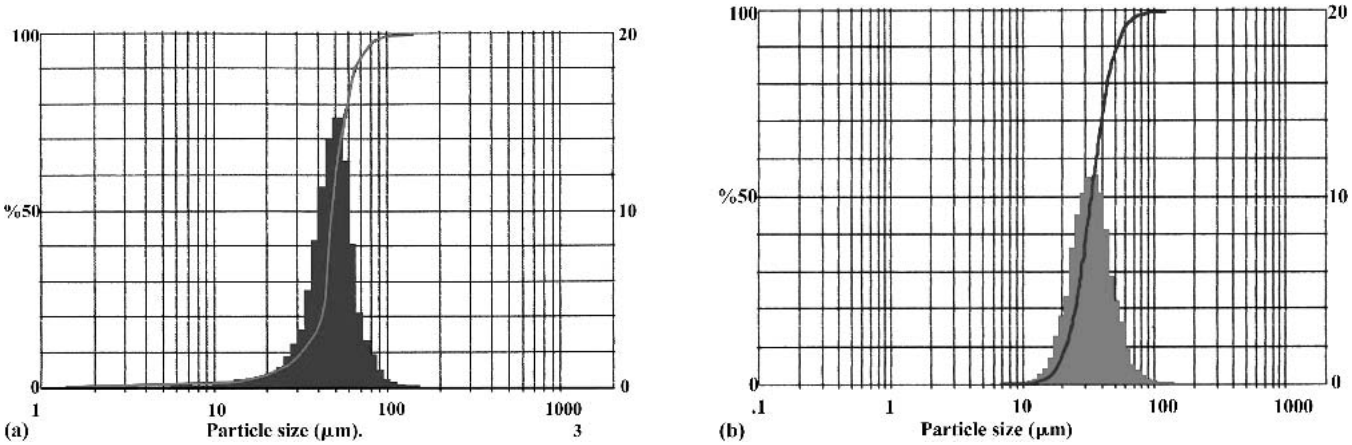

Fig. 1 Particle size distribution (frequency histograms and cumulative curves): (a) nanostructured WC-15 wt.% Co powders (Nanocarb) and (b) conventional agglomerated and sintered WC-17% Co powders (Tafa 1343 V)

and sintered WC-17 wt.% Co powders (Tafa 1343 V, Tafa Inc., Praxair Surface Technologies, Concord, NH). Particle size distribution is shown in Fig. 1(b) (average size is about 30 μm).

Standard deposition parameters were selected for spraying WC-Co conventional powders. Optimal spraying conditions for nanostructured coatings were selected using a three-level Box-Behnken factorial plan (Ref 16). Kerosene flow rate, length of the barrel positioned at the end of the torch, and spraying distance are the deposition parameters most strongly affecting the amount of energy transferred to the powders and the available time for decarburation or other chemical reactions among the species. Therefore, these three parameters were selected as variables, and varied in the ranges shown in Table 1. The oxygen flow rate was fixed at 56,634 l/h (2000 scfh). The complete Box-Benken experimental matrix can be found elsewhere (Ref 17). The following objective variables identifying composition, microstructure, and final performance of the coatings were selected for the statistical optimization: friction coefficient, fracture toughness, total wear, Vickers microhardness, porosity, and carbide retention.

Microstructural characterization of powders and coatings was performed by scanning and transmission electron microscopes (Philips XL 30 LaB_6 analytical and Philips CM 120 LaB_6 analytical, Philips-FEI Company, Eindhoven, The Netherlands). Preparation of samples was carried out by dimpling, grinding (6-3-1 μm diamond suspension paste, residual sample thickness 5 μm) and ion thinning (Baltec RES, BAL-TEC AG, Liechtenstein; 100, 8 kV double gun, 13° grazing incidence till hole and 6 kV double gun 7° for 2 h).

Phase composition (crystallinity of the matrix, stoichiometry of tungsten carbides, and formation of mixed phases) was investigated by x-ray diffraction (XRD; Siemens D500, Siemens AG, Munich, Germany; Cu Kα radiation, 30-80° 2θ range, 0.01° step width, 1 s per step acquisition time). The XRD technique (0.005° step width, 5 s per step) was also used for the determination of the average grain size of WC in the original powders, carried out by calculating the broadening [full-width at half-maximum (FWHM)] of the main peak of WC (2θ = 35.6°) and taking into account, with a Stokes deconvolution, the contribution of instrumental errors evaluated on the main peak of a quartz reference (Ref 18).

Table 1 Variation range for the three variable parameters selected for the experimental plan

	Minimum	Central	Maximum
Kerosene flow rate, l/h (gph)	22.7 (6.0)	24.6 (6.5)	26.5 (7.0)
Barrel length, cm (in)	10.16 (4)	20.32 (8)	30.48 (12)
Spraying distance, mm	360	380	400

Vickers microhardness of the coatings was evaluated by means of a Leica VMHT Vickers indenter (Leica Microsystems, Wetzlar, Germany; average of 30 measurements carried out with a 5 N normal load applied for 15 s). Dynamical indentations were also performed by CSM microhardness tester (CSM Instruments, Peseux, CH) on selected coatings, and elastic modulus was calculated from the load-displacement curves obtained by repetitive load/unload cycles (maximum load = 1 N, loading rate = 2 N/min, 15 s pause between cycles). Fracture toughness (K_{Ic}) was calculated according to Lawn-Fuller (Ref 19) and Evans-Wilshaw (Ref 20) models by measuring the length of microcracks generated at the tips of the imprint by microindentation.

Porosity of the coatings was evaluated by image analysis (Leica QWin v.2, Leica Microsystems, Wetzlar, Germany) on polished cross sections.

Finally, the tribological behavior of all coatings was investigated in terms of friction coefficient and total wear, using a Plint TE53 SLIM/8941 tribometer (Phoenix Tribology Ltd, Newbury, UK; testing time 15 min, total run 0.565 km, applied normal load on the counterbody 67 N) in the two different configurations of "block on ring" (linear contact) and "ball on ring" (punctual contact, ASTM G77 standard).

3. Results and Discussion

3.1 Computational Modeling of Gas and Powders

Profiles of temperature, pressure, velocity, and composition of the combustion gas in the torch along barrels of different length and in the external field of the jet were calculated for

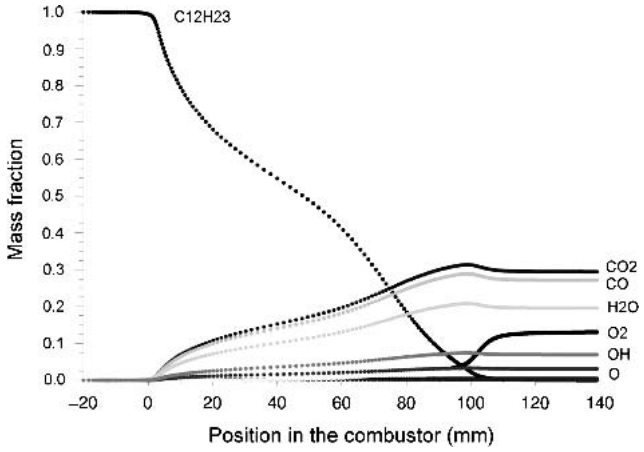

Fig. 2 Composition profiles of the oxyfuel mixture along the centerline of the torch for a kerosene flow rate of 24.6 l/h (mass fractions of OH, O_2, O, H_2O, H_2, H, CO_2, CO, and $C_{12}H_{23}$)

different operating conditions. More detailed results of the simulation can be found in Ref 15.

In the presence of oxygen, the kerosene molecule ($C_{12}H_{23}$) breaks down mainly to carbon dioxide (CO_2) or carbon monoxide (CO) and water vapor (H_2O). Atomic oxygen (O) and hydroxilic group (OH) were also considered for completeness. As a particular example, the composition of the oxyfuel mixture along the centerline of the torch was modeled for a kerosene flow rate of 24.6 l/h. Results are summarized in Fig. 2.

Temperature and velocity profiles of the combustion gas inside the HVOF torch for three different oxygen-fuel ratios (kerosene flow rates of 6.0, 6.5, and 7.0 gph corresponding to 22.7, 24.6, and 26.5 l/h) are illustrated in Fig. 3. Temperature profiles of the gas inside barrels of different length (4, 8, and 12 in., corresponding to 10.16, 20.32, and 30.48 cm, respectively) and in the external field are indicated in Fig. 4.

The thermal and dynamic behavior of WC-Co powders characterized by an average particle size of 48 μm, injected in the

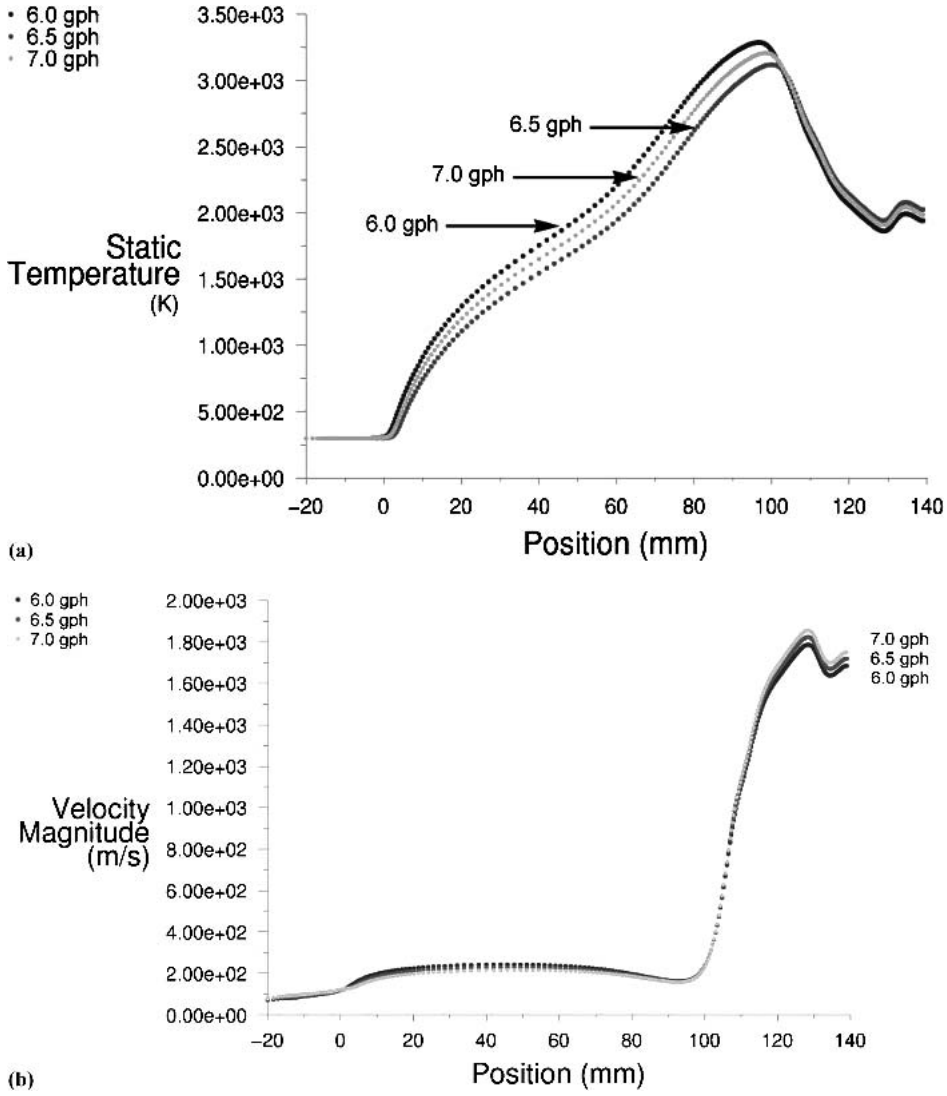

Fig. 3 Combustion gas along the torch centerline, for three different compositions of the mixture (kerosene flow rates of 6.0, 6.5, and 7.0 gph): (a) temperature profiles (K) and (b) velocity profiles (m/s)

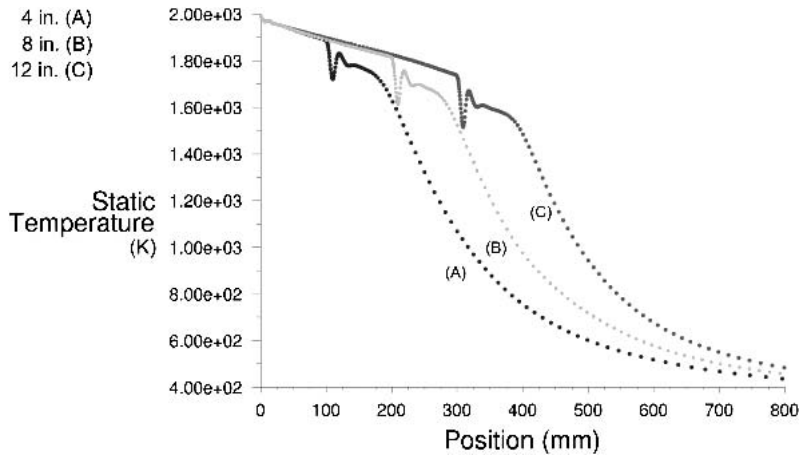

Fig. 4 Combustion gas inside barrels of different length (A: 4 in, B: 8 in, and C: 12 in, corresponding to 10.16, 20.32, and 30.48 cm, respectively) and, in the external field, simulated temperature profiles

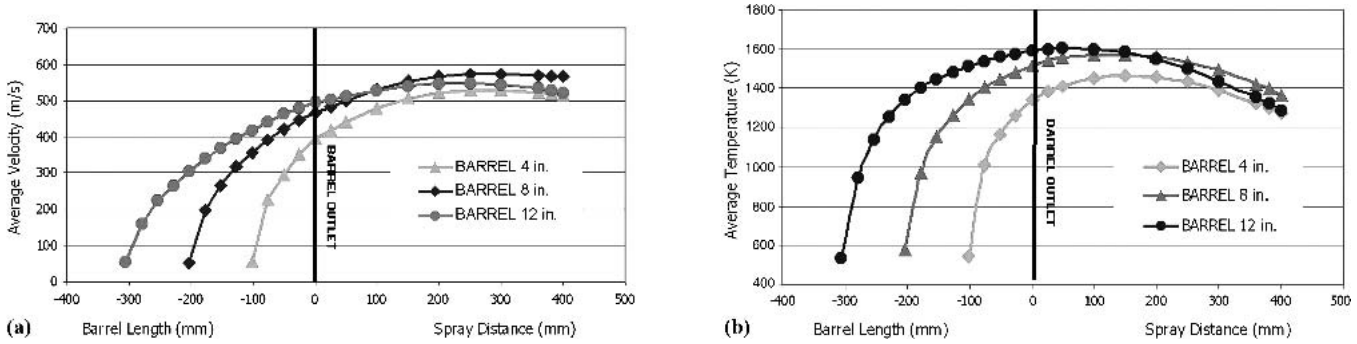

Fig. 5 WC-Co particles (48 μm average size) inside and outside barrels of different length (4, 8, and 12 in.): (a) simulation of the average axial velocity and (b) simulation of the average temperature

HVOF torch, and sprayed through the three different barrels was also investigated. Figure 5 summarizes the results of the simulation of particle velocity (Fig. 5a) and temperature (Fig. 5b) inside and outside the barrels. Information from the curves can be used to aid in selecting the spraying parameters with the goal of minimizing thermal interaction of the particles with the combustion flame (leading to minimum decarburation and grain growth) while building up coherent and adhesive coatings.

3.2 Characterization of Powders and Coatings

3.2.1 XRD Characterization: Decarburation. Scanning electron microscopy (SEM) images of Nanocarb WC 15% Co powders are shown in Fig. 6. X-ray diffraction (XRD) analyses confirmed the presence of metallic cobalt and of stoichiometric WC. An average size of 40 nm for carbide reinforcement particles was calculated by the physical broadening of the main peak of WC in XRD patterns.

Figure 7 shows typical microstructures of HVOF coatings produced by conventional (Fig. 7a) and nanosized (Fig. 7b) WC-Co powders. Low degrees of porosity (<1%) were obtained for all coatings.

The carbide distribution in Nanocarb deposits is generally more uniform than that in conventional coatings. However, the amount of crystalline growth experienced by tungsten carbide particles can differ substantially for coatings deposited in different conditions (Fig. 8a and b). In Fig. 9, XRD patterns of three representative coatings are compared. The conventional "microstructured" coating (Fig. 9a) shows an almost unaffected crystalline structure of WC; peaks related to cobalt are indistinguished under a continuous large band around 40-45°, indicating the formation of mixed amorphous phases, as often documented in the literature (Ref 21-23). Figure 9(b) (sample a in Fig. 8) gives evidence of a partial alteration of the tungsten carbide stoichiometry, indicating the presence of moderate amounts of tungsten-enriched phases (W_2C, WC_{1-x}) and of metallic W, as well as the formation of mixed η phase Co_3W_3C. Finally, pattern (c) (obtained for sample b in Fig. 8) clearly indicates that an intense decarburation process has taken place during deposition.

Decarburation of WC dissolved in the liquid cobalt is caused by the oxidation of C to CO or CO_2 with the precipitation of W_2C and of substoichiometric WC_{1-x} on the surface of WC crystals. Associated with these reactions is the probable formation of a carbon concentration gradient in the outer zone of the single carbides positioned in the external region of the agglomered particles. Nanoscale precipitates of unknown composition (possibly tungsten carbide or η mixed phase) were also de-

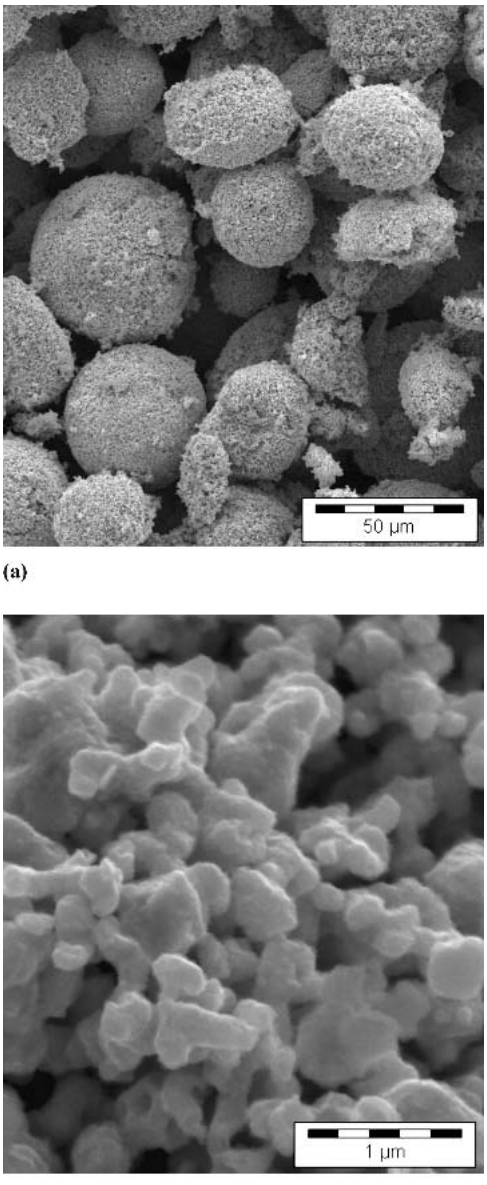

Fig. 6 SEM micrographs of commercial nano-structured WC 15 wt.% Co powders: (a) general view and (b) microstructural detail of the surface of an agglomered granule

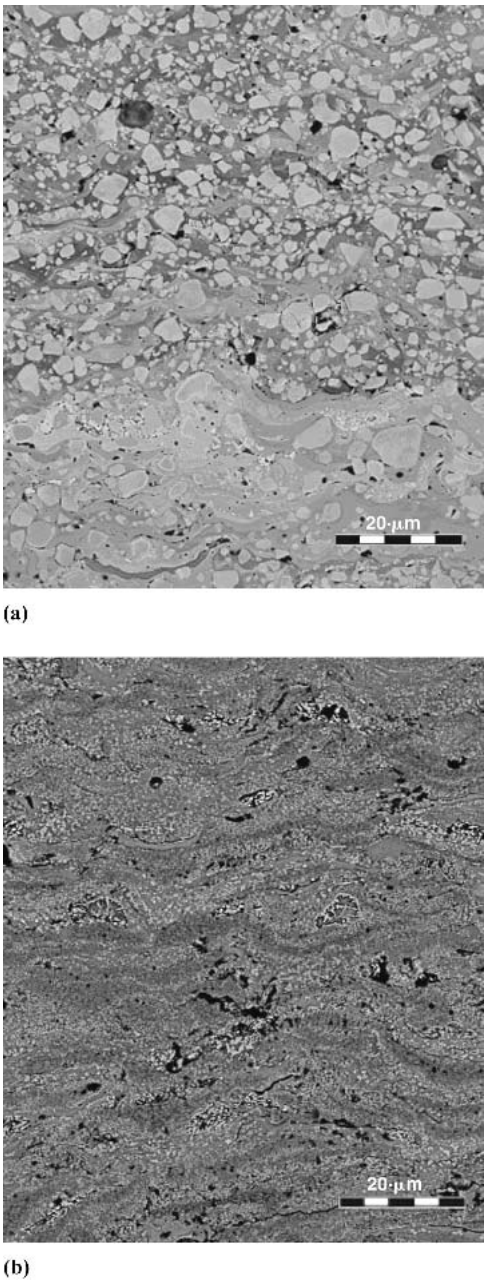

Fig. 7 Cross sections of HVOF coatings: (a) conventional WC 17% Co and (b) nanostructured WC 15% Co coating (SEM micrographs)

tected within the metallic matrix by high-resolution TEM analysis (Fig. 10). Further microstructural and microanalytical investigation is in progress.

The presence of decarburated tungsten carbide and amorphous mixed cobalt phases indicates that a certain degree of melting of the metallic matrix was reached during spraying of some of the coatings. This experimental evidence could appear in contrast with the results of the temperature simulation of the particles, reported in Fig. 5(b), where the melting temperature of cobalt (1768 K) is never reached for any of the possible barrel lengths (a maximum temperature of about 1600 K is attained at the outlet section of the 12 in. barrel). However, it is important to remember that the temperature profiles of the powders were calculated for an average particle size of 48 μm, while an important fraction of the particles (about 40%) is in fact characterized by a smaller diameter. One can therefore assume that fine particles attain on flight an almost complete degree of melting, while larger agglomerates generally remain unmelted, plastic, and deformable.

A major role is played in this direction by the residence time of the particles at the highest temperature, strictly correlated to the particle velocity and to the length of the barrel.

An "index of carbide retention" ($I_{ret.WC}$) was calculated for the deposited coatings on the basis of the relative intensities of the most intense peak of the main phases (I_{WC}, $2\theta = 35.6°$, I_{W_2C}, $2\theta = 39.4°$, and I_W, $2\theta = 41.6°$), defined as:

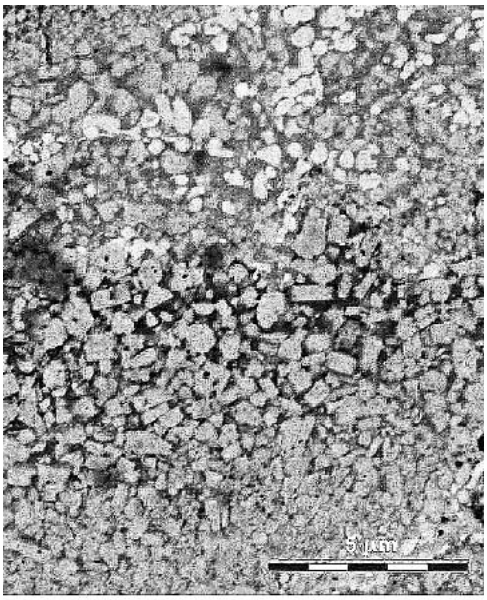

(a)

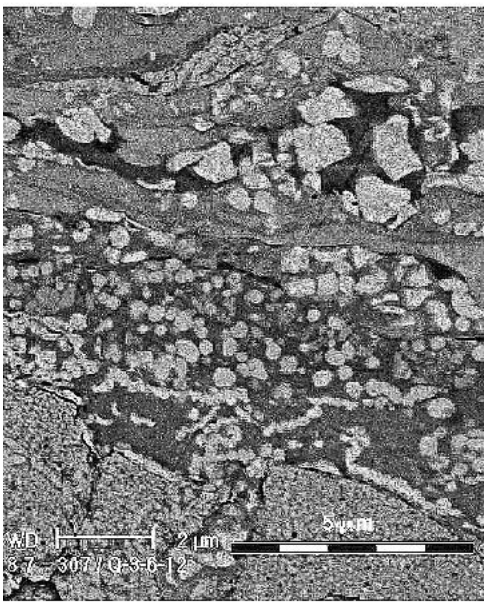

(b)

Fig. 8 Microstructural details of nanostructured coatings obtained in different conditions: (a) 380 mm spraying distance, 4 in. barrel, 22.7 l/h kerosene and (b) 380 mm, 8 in., 26.5 l/h

$$I_{\text{ret.W}} = I_{\text{WC}}/(I_{\text{WC}} + I_{\text{W}_2\text{C}} + I_{\text{W}})$$

Indices of retention varied between 0.10 and about 0.55 for nanostructured coatings, against a value of about 0.85 characterizing typical microstructured coatings.

3.2.2 Mechanical and Tribological Characterization. Vickers microhardness tests for nanostructured coatings gave VHN numbers falling in the range of 1000-1300 ± 200, with some individual values close to 1500. The best nanocoatings exhibited hardness values almost 20% higher than conventional deposits (1100 ± 180). Measurements performed on selected coatings by dynamic indentation confirmed the better performance of nanostructured coatings, which showed an average value of VHN of 1718 ± 360 as compared with a value of 1343 ± 135 for conventional WC-Co deposits.

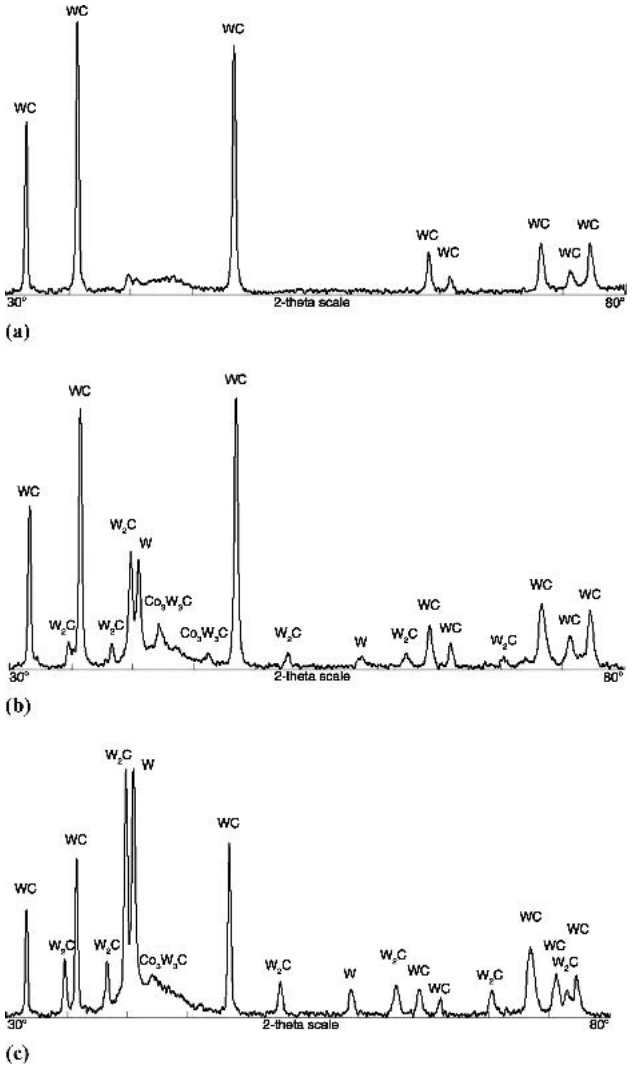

Fig. 9 XRD patterns of three representative coatings: (a) conventional coating, almost unaffected structure, (b) partially decarburized nanostructured coating, and (c) intensely decarburized nanostructured coating

Elastic moduli were calculated from the slope of the load-displacement curves obtained from the dynamical microhardness tests (Fig. 11). An average value of 413 GPa was measured for nano-coatings, about 25% above that of the microstructured coatings (309 GPa).

Fracture toughness of the coatings was also measured from indentation imprints (Fig. 12), calculated from the length of the longitudinal cracks initiated by loading the pyramidal indenter. Such cracks propagate parallel to the substrate in the cobalt matrix along matrix-reinforcement interfaces, representing the surfaces of weakest resistance. All nanostructured samples exhibited higher K_{IC} (6-10 MPa $m^{1/2}$, calculated according to the

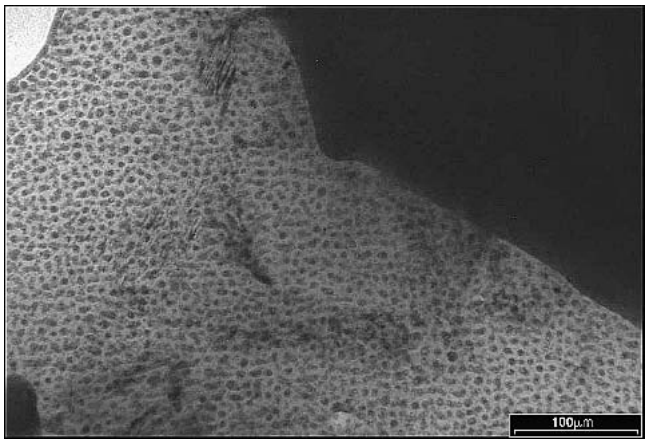

Fig. 10 Nanoscale precipitations in the metallic matrix (transmission electron microscope image)

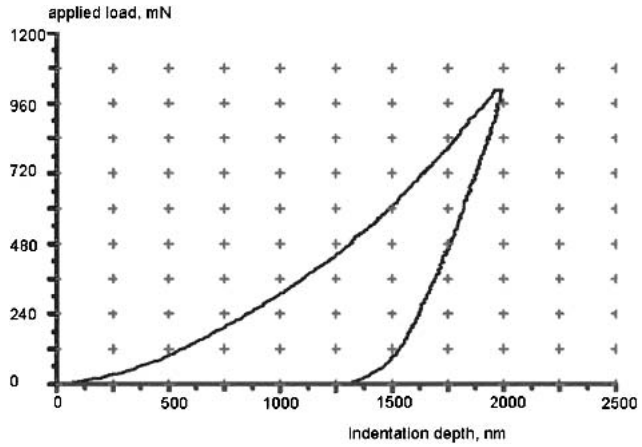

Fig. 11 Load/unload-displacement curve for the dynamical evaluation of the microhardness and of the elastic modulus of the coatings

Evans and Wilshaw model) than conventional deposits (2-3 MPa $m^{1/2}$). The smaller size of carbides and a higher degree of homogeneity of the reinforcement distribution, together with the precipitation of nanoscale hard particles from the amorphous cobalt matrix, can be responsible for the general improvement of the penetration and crack advancement resistance; in fact, in the presence of finer and more numerous carbides in the metallic matrix, longer free average paths of the crack are generated before extinction, with dissipation of higher amounts of energy.

Tribological tests also showed a clear influence of deposition parameters on abrasion resistance of nanostructured coatings. The total wear experienced by individual nano-coatings was compared with the wear of conventional microstructured coatings tested in the same operating conditions. Nanostructured coatings generally outperformed conventional deposits, showing values of total wear about two- to five-fold lower. On the other hand, fairly homogeneous values of friction coefficient in the range of 0.69-0.88 were measured for samples deposited in different conditions.

The better performance of nano-sized coatings in terms of wear resistance can be explained by observing the individual

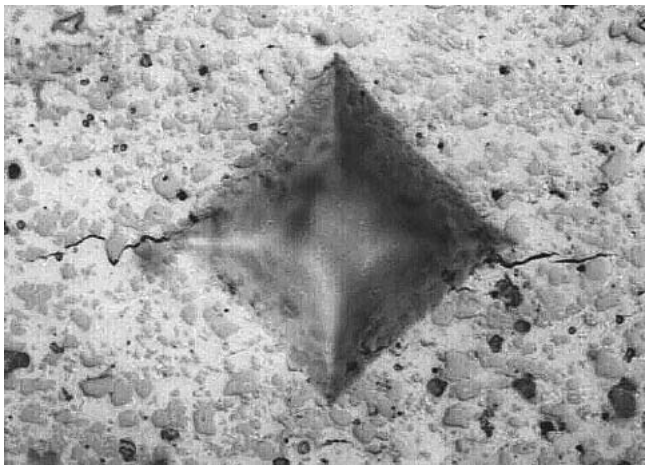

Fig. 12 Indentation of a nanostructured coating: longitudinal cracks originate at the tips of the imprint and propagate in the cobalt matrix along matrix-reinforcement interfaces. Fracture toughness of the composite coating is evaluated from the total length of the cracks.

steps of the wear process. At the beginning of the friction process, an adhesive wear mechanism is responsible for transferring part of the ductile material (cobalt) from the matrix to the surface of the alumina counterbody, thus exposing the carbide surface to the shear forces caused by the relative motion. As a consequence, hard particles are pulled out from the matrix, initiating an abrasive wear mechanism. These carbides can finally be entrapped among the sliding surfaces, thus inducing three-body abrasion damage. The larger the carbide size, the easier the pull-out effect, due to the presence of more numerous damage initiation sites (weak points characterized by high attack angles) and of more effective moments. Moreover, the abrasive action of large angular shaped particles is much more destructive than that caused by rounded nano-sized carbides. The surface appearance of typical wear tracks of conventional and nanostructured coatings, shown in Fig. 13(a) and (b), respectively, confirms the described mechanism. Parallel longitudinal marks along the sliding direction, caused by pull out of hard particles, are deeper in the microstructured coating, and the loss of material is more evident.

3.2.3 Selection of the Optimal Deposition Parameters. All above-mentioned characterization data were evaluated by statistical methods (DOE; design of experiment), and the optimal conditions for the deposition of nanostructured coatings endowed with low porosity and good hardness, toughness, and wear resistance were identified in the following parameters: spray distance, 394 mm; barrel length, 10.16 cm (4 in.); and kerosene feed rate, 22.7 l/h (6.0 gph).

The length of the barrel was found to be the most influential parameter, playing a major role in the intensity of the reinforcement decarburation by directly affecting the dwell time of the particles within the combustion flame.

Selected conditions essentially represent the optimal compromise in terms of velocity and temperature of the particles, as confirmed by the curves shown in Fig. 5; the use of a short barrel at a spraying distance of about 400 mm allows deposition of particles with a maximum temperature of about 1300 K at a minimum velocity of about 500 m/s.

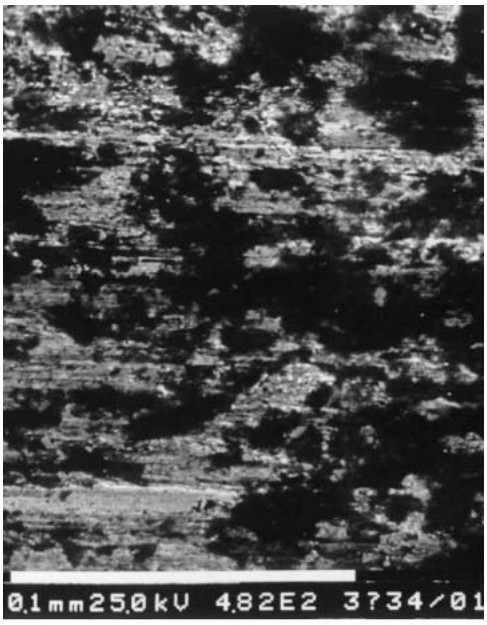

(a)

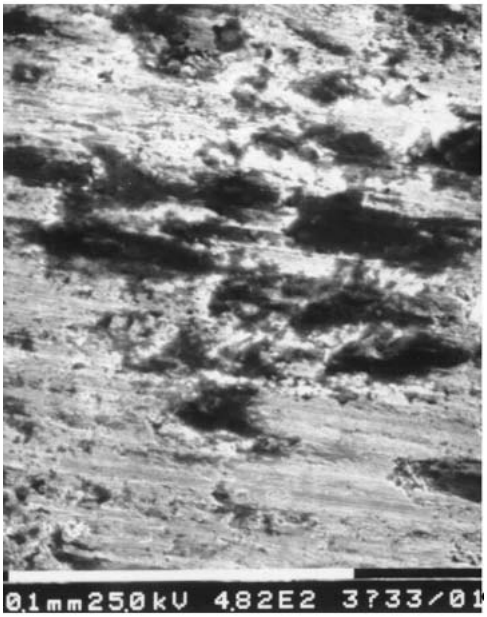

(b)

Fig. 13 Surface appearance of wear tracks of typical (a) microstructured and (b) nanostructured coatings after wear test with alumina counterbodies

The external cylindrical surface of a ring was coated in the optimized spraying conditions with a nanosized WC-15%Co deposit, and its tribological behavior was compared with that of a conventional WC-17%Co coating in the same testing configuration (ball on ring). An average friction coefficient of 0.75 and a total weight loss of 0.01 g were measured for the nanostructured coating against a friction coefficient of 0.86 and a weight loss of 0.06 g experienced in the same conditions by the conventional deposit wear tracks are shown on Fig. 13.

4. Conclusions

The computational modeling of the processes of confined combustion in a high-velocity oxygen-kerosene spraying torch and the simulation of the thermochemical and kinetic behavior of WC-Co particles in the combustion jet were used to give more complete significance to the process of statistical optimization of the operating parameters for HVOF deposition of nanostructured WC-15%Co coatings. In particular, temperature and velocity of the sprayed particles were calculated for different lengths of the external barrel, allowing adequate conditions to be identified for the minimization of particle temperature and dwell time inside the flame.

Nanocrystalline coatings were successfully deposited. In spite of the partial decarburation of the reinforcement, the mechanical and tribological behavior of optimized nanostructured coatings generally overcome those of conventional microstructured coatings of similar composition (WC-17%Co) by about 20% in terms of reduction of friction coefficient and increase in microhardness, fracture toughness, and wear resistance.

As a general trend, a negative effect of temperature and dwell time and a positive effect of particle velocity on the properties of the coatings were observed. Discussed experimental evidence suggests that the use of spraying systems based on a low thermal-high kinetic energy input could allow for optimal results. The possibility of using cold spray for spraying similar materials was already explored with some success in Ref 24. Future work will be focused in this direction.

Acknowledgments

Morphological and compositional analyses were carried out at the "Interdepartmental Laboratory of Electron Microscopy – LIME" University Roma TRE, Rome, Italy (www.lime.uniroma3.it). Dr Gregory Favaro (CSM Instruments, CH) is gratefully acknowledged for dynamical indentation measurements.

References

1. J.A. De Barro and M.R. Dorfman, The Development and Application of Chromium Plating Alternatives Using the HVOF Thermal Spray Process, *Thermal Spraying: Current Status & Future Trends,* A. Ohmori, Ed., High Temperature Soc. of Japan, Osaka, Japan, 1995, p 651-656
2. M. Gell, E.H. Jordan, Y.H. Sohn, D. Goberman, L. Shaw, and T.D. Xiao, Development and Implementation of Plasma Sprayed Nanostructured Ceramic Coatings, *Surf. Coat. Technol.,* Vol 146-147, 2001, p 48-54
3. Technical reports of the U.S.-Canadian Hard Chrome Alternatives Team, available at www.hcat.org
4. A.I. Gusev, Effects of the Nanocrystalline State in Solids, *Physics-Uspekhi,* Vol 41 (No. 1), 1998, p 49-76
5. F. Gartner, R. Bormann, T. Klassen, H. Kreye, and N. Mitra, Nanocrystalline Composites for Thermal Spray Applications, *J. Metast. Nano. Mater.,* Vol 8, 2000, p 933-940
6. M. Gell, Application Opportunities for Nanostructured Materials and Coatings, *Mater. Sci. Eng., A,* Vol 204, 1995, p 246-251
7. J. He, M. Ice, S. Dallek, and E.J. Lavernia, Synthesis of Nanostructured WC-12 Pct Co Coating Using Mechanical Milling and High Velocity Oxygen Fuel Thermal Spray, *Metall. Mater. Trans. A,* Vol 31A, 2000, p 555-564
8. B.R. Marple, J. Voyer, J.F. Bisson, and C. Moreau, Thermal Spraying of Nanostructured Cermet Coatings, *J. Mater. Proc. Technol.,* Vol 117, 2001, p 418-423

9. W.L. Oberkampf and M. Talpallikar, The Development and Application of Chromium Plating Alternatives Using the HVOF Thermal Spray Process, *J. Therm. Spray Technol.,* Vol 5 (No. 1), 1996, p 53-68
10. S. Gu, C.N. Eastwick, K.A. Simmons, and D.G. McCartney, Computational Fluid Dynamic Modeling of Gas Flow Characteristics in a High-Velocity Oxy-Fuel Thermal Spray System, *J. Therm. Spray Technol.,* Vol 10 (No. 3), 2001, p 461-469
11. K. Sakaki and Y. Shimizu, Effects of Gun Nozzle Geometry on HVOF Thermal Spray Processes, *J. Therm. Spray Technol.,* Vol 10 (No. 3), 2001, p 487-496
12. S. Eidelman and X. Yang, *Nanostruct. Mater.,* Vol 9 (No. 1-8), 1997, p 79-84
13. E.E. Khalil, *Modeling of Furnaces and Combustors,* Abacus Press, Turbridge Wells, UK, 1982, p 27-29
14. S.R. Turns, *An Introduction to Combustion,* McGraw-Hill, UK, 1996, p 372-375
15. C. Bartuli, F. Cipri, T. Valente, and N. Verdone, CFD Simulation of an HVOF Process for the Optimization of WC-Co Protective Coatings, Comp. Experimental Methods, 2003, 7 (Surface Treatment VI), p 71-83
16. F.W. Breyfogle III, *Statistical Methods for Testing, Development, and Manufacturing,* Wiley Interscience, Austin, Texas, 1992, p 255
17. C. Bartuli, T. Valente, F. Cipri, and E. Bemporad, Nanostructured Wear Resistant Coatings Deposited by HVOF, in *Surface Engineering: Coatings and Heat Treatments,* Electronic Publication on CD-ROM, ASM International, 2003, p 480-488
18. B.E. Warren, *X-Ray Diffraction,* Addison-Wesley Publishing Co., Boston, MA, 1969, p 251
19. B.R. Lawn and E.R. Fuller, Equilibrium Pennylike Cracks in Indentation Fracture, *J. Mater. Sci.,* Vol 10, 1975, p 2016-2024
20. A.G. Evans and T.R. Wilshaw, Quasi-static Solid Particle Damage in Brittle Solids: I. Observations, Analysis And Implications, *Acta Metall.,* Vol 24, 1976, p 939-956
21. H.L. de Villiers Lovelock, Powder/Processing/Structure Relationships in WC-Co Thermal Spray Coatings: A Review of the Published Literature, *J. Therm. Spray Technol.,* Vol 7 (No. 3), 1998, p 357-373
22. Y. Zhu, K. Yukimura, C. Ding, and P. Zhang, Tribological Properties of Nanostructured and Conventional WC-Co Coatings Deposited by Plasma Spraying, *Thin Solids Films,* Vol 388, 2001, p 277-272
23. D.A. Stewart, P.H. Shipway, and D.G. McCartney, Abrasive Wear Behavior of Conventional and Nanocomposite HVOF-Sprayed WC-Co Coatings, *Wear,* Vol 225-229, 1999, p 789-798
24. J. Karthikeyan, C.M. Kay, J. Lindemann, R.S. Lima, and C.C. Berndt, Cold Sprayed Nanostructured WC-Co, in *Thermal Spray 2001: New Surfaces for a New Millennium,* C.C. Berndt, K.A. Khor, and E.F. Lugsheider, Ed., ASM International, Materials Park, OH, 2001, p 383-387